Radiative one- and two-electron transitions into the empty K shell of He-like ions

Riddhi Kadrekar and L. Natarajan
Department of Physics, University of Mumbai, Mumbai 400 098, India
(Received 19 May 2011; published 12 December 2011)

The branching ratios between the single and double electron radiative transitions to empty K shell in He-like ions with $2s2p$ configuration are evaluated for 15 ions with $4 \leqslant Z \leqslant 26$ using fully relativistic multiconfiguration Dirac-Fock wavefunctions in the active space approximation. The effects of configuration interaction and Breit contributions on the transition parameters have been analyzed in detail. Though the influence of Breit interaction on the electric dipole allowed one-electron radiative transitions is negligible, it substantially changes the spin-forbidden rates and the two-electron one-photon transition probabilities. Also, while the single electron transition rates are gauge independent, the correlated double-electron probabilities are found to be gauge sensitive. The probable uncertainties in the computed transition rates have been evaluated by considering the line strengths and the differences between the calculated and experimental transition energies as accuracy indicators. The present results are compared with other available experimental and theoretical data.

DOI: 10.1103/PhysRevA.84.062506 PACS number(s): 32.30.−r

I. INTRODUCTION

During recent years, investigation on the various properties of highly charged ions has received much attention. The x-ray spectra of He-like ions, especially from carbon to iron, provide valuable information on the temperature diagnostics of astrophysical and laboratory plasmas. Precise transition properties can act as reference data for the charge state distribution and average charge of plasma. The doubly excited states of $2s2p$ configuration in He-like ions can decay to the $1s2s$ states either by one-electron one-photon transition (OEOP) or to the $1s^2$ ground configuration through two-electron one-photon (TEOP) transition. Though the former decay process has been both experimentally and theoretically investigated extensively for many He-like ions, experimental investigations on the less-intense latter process are scarce, thereby placing added importance on the systematic evaluation of theoretical data. The double photoionization cross sections of K shell and the observation of TEOP transitions in Mg, Al, and Si using synchrotron radiation have been very recently reported by Hoszowska *et al.* [1,2]. Accurate evaluation of measurable quantities, such as lifetimes, fluorescence yields, ionization cross sections, does require the x-ray rates from both the processes.

The OEOP x-ray satellites emitted from doubly excited states have been observed in laser-produced plasmas [3–10], ion-solid and ion-atom collisions [11–13], Z pinch experiments [14], laser-imploded microballoons [15,16], electron cyclotron ion source [17,18], tokamak [19], beam foil spectroscopy [20,21], and solar flares [22]. On the theoretical side, most of the previous data on OEOP transitions from doubly excited He-like ions are largely on nonrelativistic models, and relativistic calculations using various methods exist only for a few elements. Mosnier *et al.* [21] have carried out multiconfiguration Dirac-Fock (MCDF) calculations on H-like to Be-like silicon. Chen has performed explicit calculations on the doubly excited states of $2l2l'$ and $2l3l'$ configurations in some He-like ions using nonrelativistic and relativistic Hartree-Fock models with the inclusion of Breit interaction [23]. Relativistic many body perturbation calculations on He-like Mg are also available in literature [9]. Recently modified Z expansion calculations with relativistic corrections on the various states of $2lnl'$ and $1s2lnl'$ configurations have been reported by Goryayev *et al.* [24].

The TEOP satellite x-rays from variously ionized systems with closed K shell have been experimentally investigated for some ions using synchrotron radiation [2,25], ion-atom collisions [26], electron beam ion trap [27–29], and laser produced plasmas [30]. However, to the best of our knowledge, the x-ray emission due to correlated two electron jump from states of $2s2p$ configuration to empty K shell has not been experimentally investigated so far apart from a few He-like ions [11,20] and theoretically less intensively studied. Though nonrelativistic data on $2s2p$-$1s^2$ transitions are available in literature [31,32], fully relativistic calculations have so far not been carried out.

The present work reports a detailed study of both OEOP and TEOP transitions from doubly excited $2s2p$ configuration in He-like ions. Restricting to the most cosmically abundant elements in the range $4 \leqslant Z \leqslant 26$, the calculations have been computed in the relativistic configuration interaction formalism (RCI), which uses correlated MCDF wavefunctions and includes Breit interaction and quantum electrodynamics (QED) effects. The finite nuclear size has been included in the calculations by considering a two-parameter Fermi charge distribution. The electron-electron correlation has been considered in the active space approximation. The purpose of the present study is to investigate the contribution from two-electron one-photon transitions to the dominating main channel of radiative decay for a most accurate description of two-electron configurations with empty K shell. An attempt has also been made to analyze the importance of Breit interaction on OEOP and TEOP transitions. The calculations have been carried out using the GRASP2K code [33], which is a modification of GRASP92 code [34].

II. NUMERICAL PROCEDURE

In a multiconfiguration relativistic calculation, the configuration state functions (CSFs) are antisymmetrized sum of product of Dirac spinors. A linear combination of these CSFs is

then used in the construction of atomic state functions (ASFs) with the same J and parity,

$$\Psi_i(J^P) = \sum_{\alpha=1}^{n_{\rm CSF}} c_{i\alpha}\Phi(\Gamma_\alpha J^P), \quad (1)$$

where $c_{i\alpha}$ are the mixing coefficients for state i and $n_{\rm CSF}$ are the number of CSFs included in the evaluation of ASF. The Γ_α represents all the one-electron and intermediate quantum numbers needed to define the CSFs and the configuration mixing coefficients are obtained through the diagonalization of the Dirac-Coulomb Hamiltonian

$$\mathbf{H}_{DC} = \sum_i \left[c\alpha_i \cdot \mathbf{p}_i + (\beta - 1)c^2 - \frac{Z}{\mathbf{r}}\right] + \sum_{i>j}\frac{1}{\mathbf{r}_{ij}}. \quad (2)$$

Once a set of radial orbitals and the expansion coefficients are optimized for self-consistency, RCI calculations can be performed by including higher-order interactions in the Hamiltonian. The most important of these is the transverse photon interaction

$$\mathbf{H}_{\rm trans} = \sum_{i,j}^{N}\left[\frac{\alpha_i \cdot \mathbf{p}_i \cos(\omega_{ij})}{\mathbf{r}_{ij}} + (\alpha_i \cdot \nabla_i)(\alpha_j \cdot \nabla_j)\frac{\cos(\omega_{ij}) - 1}{\omega_{ij}^2 \mathbf{r}_{ij}}\right] \quad (3)$$

and the mixing coefficients may be reevaluated by diagonalizing the Dirac-Coulomb-Breit Hamiltonian matrix. The dominant QED corrections comprise self energy and vacuum polarization. In the present code, the self energy in hydrogenic systems with a rough estimate of electron screening is evaluated using the one-electron values available in literature [35]. The second-order (Uehling) and fourth-order (Kallen Sabry) vacuum polarization potentials [36] are included as perturbation corrections. The theoretical background necessary for the evaluation of structure parameters using MCDF wavefunctions, including higher-order corrections is described in detail in literature [34,37–39].

The construction of the atomic state functions using systematic expansion of the orbitals in the active space has been discussed in our earlier studies [40,41]. In this method, the electrons from the occupied orbitals are excited to unoccupied orbitals in the active set. Since the orbitals with the same principal quantum number n have near similar energies, the active set is expanded in layers of n and the $\{nl\}$ set in general includes all the orbitals with $l = 0$ to $n - 1$. Our calculations showed that OEOP transition parameters converged well with $\{nl\}$ set consisting of $n = 1$ to 4 and $l = 0$ to 3. Correlation from higher orbital set with $n > 4$ did not contribute to the converged observables. However, the TEOP transitions being correlation sensitive, the enhanced effects of correlation are systematically considered by expanding the active space from $\{1s, 2s, 2p\}$ to the set that consisted of all orbitals with $n = 1$ to 8 and $l = 0$ to 3 so as to ensure maximum correlation, stability, and convergence of the observables.

The correlation contribution was evaluated by considering single and double (SD) excitations of electrons from the reference configurations to the orbitals in the active set. We did separate calculations to evaluate the transition parameters of OEOP and TEOP processes. However, the procedure followed in the generation of CSFs was the same in both the cases. We first generated Dirac-Fock wavefunctions in extended optimal level (EOL) scheme for the initial doubly excited $2s2p$ and final $1s2s$ configurations. In the EOL method, the radial functions and the mixing coefficients are determined by optimizing the energy functional, which is the weighted sum of the energy values corresponding to a set of $(2j + 1)$ eigenstates. We then considered limited expansion and generated 24 CSFs by allowing SD excitations of electrons from the reference configurations with four relativistic subshells and used these optimized CSFs to evaluate the transition parameters. As this procedure led to better optimized wavefunctions than the Dirac-Fock (DF) functions, all our investigations on the effects of correlation and higher-order corrections were carried out with respect to this 24 CSFs data. Then we expanded the active space by considering the first layer of the set with $n = 3$ and $l = 0$ to 2 virtual shells and optimized the orbital functions while $1s$, $2s$, and $2p$ orbitals were kept fixed. Thus, by gradually expanding the size of the active space until the convergence of the observable is obtained, the two sets of SD excitation calculations, one with only correlation and the other with contributions from higher-order corrections to the correlated functions were repeated for each step by step multiconfiguration expansion taking care of the convergence criterion on the orbitals (10^{-8}). To ensure numerical stability and to reduce processing time, during each layer by layer expansion of the virtual orbitals, only the newly added orbitals were optimized while the previously generated orbitals were kept frozen. The optimized orbitals thus generated were used in the evaluation of MCDF energies and rates. In the subsequent RCI calculations, we recalculated the mixing coefficients with a frozen radial set. As the ASFs of initial and final states consisted of CSFs built from different orthonormal sets, they were first transformed to become bi-orthonormal in the transition rates calculations.

III. RESULTS AND DISCUSSION

The RCI excitation energies along with the observed level energies of $1s2s$ and $2s2p$ configurations are listed in Table I for some He-like ions. All the energies are given with respect to $1s^2\ ^1S_0$ ground state. While the level energies of $1s2s$ configuration listed in the table correspond to OEOP calculations with orbital set $\{nl, l \leqslant n - 1\}$ up to $n = 4$, the excitation energies of the fine structure states of $2s2p$ configuration and the ground state are taken from TEOP calculations with $\{nl, l \leqslant n - 5\}$ up to $n = 8$. The level energies of He-like ions compiled in NIST database are mainly theoretical and hence we have used some auxiliary data, $1s2s(^3S_1, ^1S_0)$–$1s^2(^1S_0)$ observed transition energies, to evaluate the final experimental energies of the doubly excited states. The auxiliary data were taken from NIST's atomic spectra bibliography database [42], and to limit the number of references, these references are not listed in this work. The blanks in the table imply that observed energies are not available in literature. Most of the experimental data reported for $2s2p(\ ^3P_0, ^3P_1, ^3P_2)$–$1s2s(^3S_1)$ transitions are unresolved and hence the computed ^3P -level energies listed in the table correspond to the average values of the three fine structure states. The calculated excitation energies deviate from the experimental energies by 0.4% at

TABLE I. LSJ energies in cm^{-1} for excited states of $1s2s$ and $2s2p$ configurations of He-like ions. Also listed are the experimental level energies. The ^3P denotes the average of $^3P_0$, $^3P_1$, and $^3P_2$ states. All energies in cm^{-1} are displayed with respect to $1s^2\ ^1S_0$ ground state.

Levels		Present	Expt.	Present	Expt.	Present	Expt.
		$Z = 4$		$Z = 7$		$Z = 10$	
$1s2s$	$^3S_1$	951 859.33	956 506	3380 814.62	3 385 856	7 294 549.81	7 298 737
	$^1S_0$	977 049.37	981 175	3 435 178.08	3 439 275	7 378 529.70	
$2s2p$	$^3P_0$	2 225 210.20		7 335 544.38		15 417 087.17	
	$^3P_1$	2 225 232.05		7 335 782.94		15 418 130.60	
	$^3P_2$	2 225 282.82		7 336 307.09		15 420 411.88	15 427 635
	^3P	2 225 241.69	2 229 904	7 335 878.14	7 342 178	15 418 543.22	15 427 624
	$^1P_1$	2 264 733.22	2 268 434	7 413 520.36	7 419 375	15 535 249.41	
		$Z = 5$		$Z = 8$		$Z = 12$	
$1s2s$	$^3S_1$	1 596 737.47	1 601 532	4 520 235.83	4 525 285	10 730 717.77	10 734 221
	$^1S_0$	1 631 575.75	1 635 710	4 584 425.04	4 588 422	10 834 719.19	10 836 000
$2s2p$	$^3P_0$	3 598 951.78		9 698 863.17		22 460 047.61	
	$^3P_1$	3 599 009.15		9 699 279.41		22 462 231.64	
	$^3P_2$	3 599 138.70		9 700 189.12		22 467 067.97	
	^3P	3 599 033.21	3 604 020	9 699 443.90	9 706 364	22 463 115.41	22 467 179
	$^1P_1$	3 651 122.06	3 656 400	9 790 004.87	9 794 857	22 606 501.33	22 508 177
		$Z = 6$		$Z = 9$		$Z = 26$	
$1s2s$	$^3S_1$	2 406 421.31	2 411 271	5 824 758.84	5 829 613	53 520 195.24	53 527 459
	$^1S_0$	2 450 999.10	2 455 026	5 898 818.00	5 901 900	53 775 739.07	
$2s2p$	$^3P_0$	5 302 388.90		12 392 591.56		109 279 618.13	
	$^3P_1$	5 302 513.57		12 393 268.87		109 317 968.58	
	$^3P_2$	5 302 790.32		12 394 747.04		109 444 301.05	
	^3P	5 302 564.26	5 307 891	12 393 535.82	12 398 189	109 347 295.92	109 260 007
	$^1P_1$	5 367 377.37	5 371 668	12 497 113.51	12 500 382	109 729 920.79	

$Z = 4$ and the difference decreases with increasing Z reaching 0.01% at $Z = 26$.

In Table II we give the RCI energies of the various OEOP transitions from states of $2s2p$ configuration. The first row of each ion gives the present energies and the rest of the rows give the high-resolution measurements [3–9,12–16,19–22] and other calculated energies. As the paper aims to analyze the influence of relativistic configuration interaction on the transition parameters, to limit the length of the table, we have included only available relativistic data [9,20,21,23,24]. Taking into account the experimental errors, we observe that our values are in general in very good agreement with the experimental data for Be [5], B [5,6], C [5], N [5], O [5], F [20], Ne [14], Mg [3,4,7,9], Si [3,8,12,21], Ar [16], Ti [19], and Fe [13,22] and differ by a maximum of 2 eV except for Si [15] and Ti [19]. It may be mentioned here that some of the experimental energies compared in the table are either graphical representations or unresolved ^3P-^3S transition energies. Though Table II does not list the earlier nonrelativistic (NR) data calculated using different models [4–7,18,19,31], we notice that our energies in general compare well with the NR values except for Ti [19]. The present energies are in good agreement with the Hartree-XR values of Trabert *et al.* for F [20], the many body perturbation data for Mg [9], and the MCDF energies of Mosnier *et al.* [21] for Si. Our energies compare exceedingly well with the Multiconfiguration Z energies of Goryayev *et al.* [24] for all the ions considered in this work.

As mentioned earlier, the ASFs with 24 CSFs generated from SD excitation of orbitals in the set $\{1s,2s,2p\}$ and optimized on various terms constituted a better basis than monoconfiguration functions, the enhanced effect of correlation on the OEOP transition energies from the set $\{nl\}$ with $n = 1$ to 4 and $l = 0$ to 3 with respect to the limited 24 CSFs set is analyzed in Fig. 1. The correlation contribution increases the energies of transitions to $1s2s\ ^1S_0$ state and decreases the transition energies to $^3S_1$ state and is nearly the same for ions with $Z > 10$. The correlation effect changes the energies of allowed transitions by 0.2 to 0.4 eV, while it is 1.4 eV for forbidden transitions.

Figure 2 displays the variations in the energies of OEOP transitions due to Breit interactions. It is seen from the figure that in contrast to correlation contribution, the Breit interaction decreases the $^1P_1$-$^1S_0$ and $^3P_1$-$^1S_0$ transition energies, whereas it very marginally increases the transition energies to $^3S_1$ state. This is due to the fact that while the Breit interaction reduces the binding energies of the various states of $2s2p$ configuration and also $^1S_0$ state of $1s2s$ configuration, it slightly increases the energies of $^3S_1$ state and this makes the transition energies marginally more than MCDF energies without Breit interaction.

The length and velocity gauges rates are in excellent agreement with each other for the various transitions to $^1S_0$ and $^3S_1$ states and the ratios of RCI dipole allowed rates in length and velocity forms (A_l/A_v) vary from 0.999 to 1.001, while the A_l/A_v values of the spin forbidden rates range from 0.997 to 1.001 and 0.999 to 1.04 for $^3P_1$-$^1S_0$ and $^1P_1$-$^3S_1$ transitions, respectively. In Table III we list the length gauge RCI rates along with the Breit interaction included MCDF rates of Chen for Cr [23], the relativistic many body perturbation rates for Mg [9], and the MZ rates of Goryayev *et al.* [24].

TABLE II. RCI energies in eV of the one-electron radiative transitions from states of $2s2p$ configuration in He-like ions. Also included are the earlier experimental and available relativistic energies. The symbol * corresponds to unresolved energies.

		Energy(eV)					
Z		$^3P_1$-$^1S_0$	$^1P_1$-$^1S_0$	$^3P_0$-$^3S_1$	$^3P_1$-$^3S_1$	$^1P_1$-$^3S_1$	$^3P_2$-$^3S_1$
4		154.75	159.65	157.87	157.87	162.77	157.88
	Expt.				158.02[*a]		
5		243.92	250.39	248.24	248.24	254.71	248.26
	Expt.				248.46[*a]		
					248.46[*b]		
	Theory				248.48[*b]		
6		353.54	361.59	359.05	359.07	367.12	359.10
	Expt.		361.86[a]		359.37[*a]		
	Theory	353.63[c]	361.35[c]	359.04[c]	359.05[c]	366.77[c]	359.09[c]
7		483.61	493.26	490.32	490.35	500.00	490.42
	Expt.		493.80[a]		490.85[*a]		
	Theory	483.72[c]	493.04[c]	490.30[c]	490.33[c]	499.66[c]	490.40[c]
8		634.16	645.42	642.07	642.12	653.38	642.23
	Expt.		645.95[a]		642.80[*a]		
	Theory	634.28[c]	645.23[c]	642.05[c]	642.10[c]	653.05[c]	642.21[c]
9		805.21	818.10	814.31	814.39	827.28	814.58
	Expt.				813.55[*d]		
	Theory	805.33[c]	817.92[c]	814.29[c]	814.37[c]	826.96[c]	814.56[c]
			818.92[d]		815.16[*d]		
10		996.79	1011.32	1007.07	1007.20	1021.73	1007.48
	Expt.				1007.86[*e]		
	Theory	996.92[c]	1011.2[c]	1007.0[c]	1007.2[c]	1021.4[c]	1007.5[c]
12		1441.64	1459.54	1454.26	1454.53	1472.43	1455.13
	Expt.	1442.92[f]	1461.16[f]		1455.71[*f]		
			1460.81[g]		1456.01[*g]		
			1460.47[h]		1455.33[*h]		1456.19[h]
			1460.37[i]	1445.18[i]	1455.45[i]		1456.05[i]
	Theory	1441.8[c]	1459.4[c]	1454.2[c]	1454.5[c]	1472.1[c]	1455.1[c]
			1460.44[i]	1455.30[i]	1455.55[i]		1456.15[i]
			1460.45[i]	1455.16[i]	1455.43[i]		1456.03[i]
13		1694.98	1714.61	1708.75	1709.13	1728.76	1709.95
	Theory	1695.1[c]	1714.5[c]	1708.7[c]	1709.1[c]	1728.5[c]	1709.9[c]
14		1968.97	1990.39	1983.88	1984.39	2005.80	1985.52
	Expt.		1991.44[g]				
			1991.7[j]				1985.8[j]
			1992[k]	1984[k]	1985[k]		1986[k]
			1990.65[l]		1985.31[l]		
			1991.44[m]		1989.85[*m]		
	Theory	1969.1[c]	1990.3[c]	1983.9[c]	1984.4[c]	2005.5[c]	1985.5[c]
		1968.71[j]	1991.44[j]	1984.08[j]	1984.58[j]		1985.74[j]
18		3272.44	3301.56	3291.69	3293.02	3322.15	3296.26
	Expt.		3304.58[n]				3299.39[n]
	Theory	3272.6[c]	3301.5[c]	3291.7[c]	3293.0[c]	3321.9[c]	3296.2[c]
20		4049.34	4082.89	4070.64	4072.60	4106.15	4077.66
	Theory	4049.5[c]	4082.8[c]	4070.6[c]	4072.6[c]	4105.9[c]	4077.6[c]
22		4910.30	4948.84	4933.54	4936.28	4974.83	4943.89
	Expt.		4953.96[o]				4949.61[o]
	Theory	4910.5[c]	4948.8[c]	4933.5[c]	4936.3[c]	4974.6[c]	4943.9[c]
24		5855.80	5900.12	5880.91	5884.60	5928.91	5895.66
	Theory	5852.4[c]	5900.1[c]	5880.9[c]	5884.6[c]	5928.7[c]	5895.7[c]

TABLE II. (*Continued*)

		Energy(eV)					
Z		$^3P_1$-$^1S_0$	$^1P_1$-$^1S_0$	$^3P_0$-$^3S_1$	$^3P_1$-$^3S_1$	$^1P_1$-$^3S_1$	$^3P_2$-$^3S_1$
26		6886.41	6937.52	6913.32	6918.10	6969.20	6933.77
	Expt.		6942[p]		6910[*q]		
	Theory	6886.7[c]	6937.6[c]	6913.4[c]	6918.1[c]	6969.0[c]	6933.8[c]

[a]Reference [5].
[b]Reference [6].
[c]Reference [24].
[d]Reference [20].
[e]Reference [14].
[f]Reference [4].
[g]Reference [3].
[h]Reference [7].
[i]Reference [9].
[j]Reference [21].
[k]Reference [8].
[l]Reference [12].
[m]Reference [15].
[n]Reference [16].
[o]Reference [19].
[p]Reference [22].
[q]Reference [13].

The present rates for Cr and Mg compare well with the earlier relativistic rates. Our rates for allowed transitions are in very good agreement with the MZ rates [24]. While our values for $^3P_1$-$^1S_0$ transition exceed the MZ rates [24] by 2 to 6%, they are smaller than the MZ results for $^1P_1$-$^3S_1$ transition.

Our calculations show that only for light elements ($Z < 12$), the difference between the length and velocity gauges rates due to large orbital set is 3 to 4%. However, the nature of contributions from correlation to the length gauge rates is the same as that of the velocity gauge rates. It reduces both length and velocity forms rates of $^3P_{0,1,2}$-$^3S_1$ transitions and enhances the spin forbidden as well $^1P_1$-$^1S_0$ allowed transition rates. Its contribution decreases with increasing Z. In Fig. 3, we give the percentage contribution to the length gauge rates from large correlation configurations with respect to limited 24 CSFs set.

A detailed analysis of Breit contribution to OEOP rates show that the influence of Breit interaction on the length and velocity gauges rates for the allowed transitions is nearly the same, whereas the contribution to forbidden transitions differ by ∼1% for small Z and is almost the same for $Z > 10$. In Fig. 4, we plot the contributions from Breit interaction to the length gauge E1 rates. It is clear from the figure that the Breit contribution to allowed E1 rates is negligible whereas its influence on the spin-forbidden rates is 6% and ∼9% at $Z = 4$ for $^3P_1$-$^1S_0$ and $^1P_1$-$^3S_1$ transitions, respectively, and decreases with increasing Z reaching nearly 1% at $Z = 26$ for both the transitions.

The RCI energies and length gauge rates of TEOP transitions from $^1P_1$ and $^3P_1$ states of $2s2p$ configurations are listed in Table IV. The available nonrelativistic data [31,32] and the experimental observations of Trabert *et al.* for F along with their calculated energies [20] are included in the table. Also

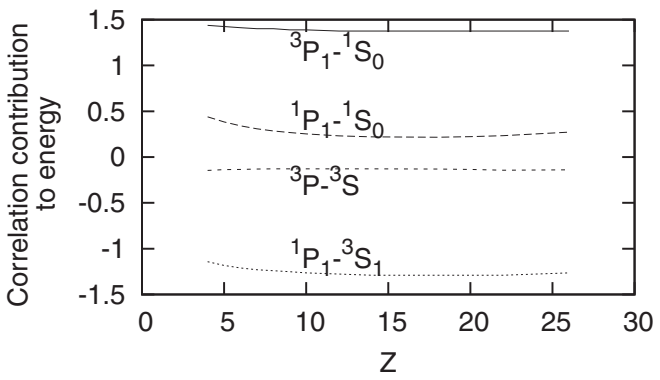

FIG. 1. Correlation contributions to the energies in eV of the $2s2p$-$1s2s$ fine structure lines in He-like ions.

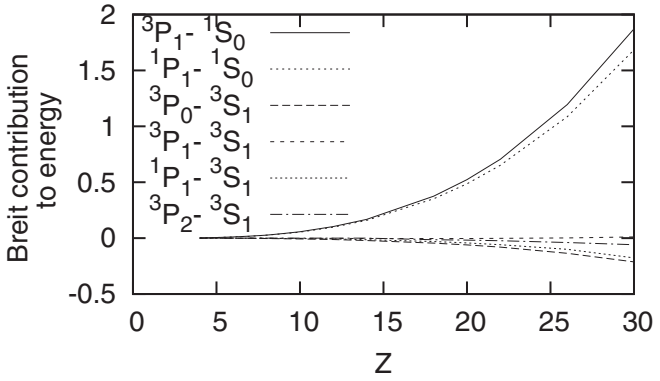

FIG. 2. Breit contribution to the energies in eV of the $2s2p$-$1s2s$ fine structure lines in He-like ions.

TABLE III. RCI length gauge rates (A_l) in sec^{-1} of the one-electron radiative transitions from states of $2s2p$ configuration in He-like ions. Also listed are the other available relativistic rates. The numbers in the parentheses are powers of ten.

		x-ray rates A_l					
Z		$^3P_1$-$^1S_0$	$^1P_1$-$^1S_0$	$^3P_0$-$^3S_1$	$^3P_1$-$^3S_1$	$^1P_1$-$^3S_1$	$^3P_2$-$^3S_1$
4		1.509(5)	1.384(11)	1.285(11)	1.285(11)	9.663(4)	1.285(11)
5		1.358(6)	3.517(11)	3.284(11)	3.284(11)	9.442(5)	3.283(11)
6		8.148(6)	7.459(11)	7.021(11)	7.020(11)	6.045(6)	7.016(11)
	Ref. [24]	7.66(6)	7.57(11)	7.10(11)	7.11(11)	8.17(6)	7.11(11)
7		3.724(7)	1.401(12)	1.330(12)	1.330(12)	2.880(7)	1.328(12)
	Ref. [24]	3.48(7)	1.42(12)	1.34(12)	1.34(12)	3.69(7)	1.34(12)
8		1.385(8)	2.413(12)	2.305(12)	2.304(12)	1.110(8)	2.301(12)
	Ref. [24]	1.29(8)	2.44(12)	2.32(12)	2.32(12)	1.37(8)	2.33(12)
9		4.417(8)	3.893(12)	3.739(12)	3.736(12)	3.634(8)	3.733(12)
	Ref. [24]	4.13(8)	3.93(12)	3.77(12)	3.77(12)	4.35(8)	3.77(12)
10		1.246(9)	5.964(12)	5.755(12)	5.751(12)	1.046(9)	5.744(12)
	Ref. [24]	1.17(9)	6.02(12)	5.79(12)	5.80(12)	1.22(9)	5.80(12)
12		7.471(9)	1.246(13)	1.211(13)	1.210(13)	6.466(9)	1.208(13)
	Ref. [9]		1.25(13)	1.22(13)	1.21(13)		1.21(13)
	Ref. [9]		1.30(13)	1.28(13)	1.28(13)		1.28(13)
	Ref. [24]	7.03(9)	1.26(13)	1.22(13)	1.22(13)	7.33(9)	1.22(13)
13		1.636(10)	1.720(13)	1.678(13)	1.675(13)	1.433(10)	1.672(13)
	Ref. [24]	1.54(10)	1.74(13)	1.69(13)	1.69(13)	1.60(10)	1.69(10)
14		3.375(10)	2.318(13)	2.268(13)	2.262(13)	2.983(10)	2.259(13)
	Ref. [24]	3.19(10)	2.35(13)	2.29(13)	2.28(13)	3.31(11)	2.29(13)
18		3.818(11)	6.346(13)	6.285(13)	6.238(13)	3.465(11)	6.246(13)
	Ref. [24]	3.63(11)	6.47(13)	6.36(13)	6.33(13)	3.75(11)	6.38(13)
20		1.034(12)	9.646(13)	9.628(13)	9.509(13)	9.472(11)	9.554(13)
	Ref. [24]	9.86(11)	9.87(13)	9.76(13)	9.67(13)	1.01(12)	9.81(13)
22		2.500(12)	1.404(14)	1.416(14)	1.388(14)	2.306(12)	1.402(14)
	Ref. [24]	2.39(12)	1.44(14)	1.44(14)	1.42(14)	2.45(12)	1.45(14)
24		5.477(12)	1.972(14)	2.012(14)	1.954(14)	5.079(12)	1.990(14)
	Ref. [23]		1.948(14)	2.004(14)	1.948(14)		1.983(14)
	Ref. [24]	5.24(12)	2.04(14)	2.05(14)	2.00(14)	5.38912)	2.07(14)
26		1.100(13)	2.683(14)	2.780(14)	2.666(14)	1.025(13)	2.744(14)
	Ref. [24]	1.06(13)	2.79(14)	2.84(14)	2.74(14)	1.08(13)	2.87(14)

listed is the experimental observation of Tawara and Richard [11] for Ar. Our energies compare well with experimental as well Hartree-XR calculations of Trabert *et al.* [20] and are in reasonable agreement with the experimental energies of Tawara and Richard [11]. The present energies differ considerably from the energies of Safronova *et al.* [31] and compare fairly well with the calculated energies of Mukherjee *et al.* [32]. While Safronova *et al.* [31] have used lowest order perturbation method with one-electron Coulomb functions, Mukherjee *et al.* [32] have considered variational principle

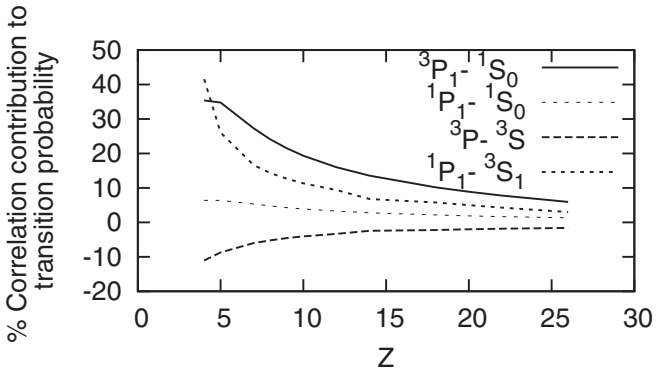

FIG. 3. Percentage difference in correlation to the length gauge rates of $2s2p$-$1s2s$ transitions from large orbital set with respect to limited (24 CSFs) set in He-like ions.

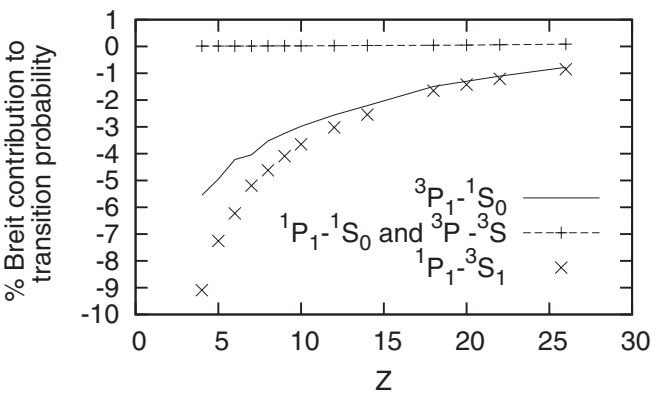

FIG. 4. Breit contribution to length gauge rates. The legends are the same as in Fig. 3.

TABLE IV. RCI energies in eV, length gauge (A_l) rates in sec^{-1} of two-electron one-photon transitions from states of $2s2p$ configuration in He-like ions. The available experimental and other theoretical data are also listed. The numbers in the parentheses are powers of ten.

		$^3P_1$-$^1S_0$		$^1P_1$-$^1S_0$	
Z		Energy	Rate	Energy	Rate
4		275.878	1.296(3)	280.777	8.319(8)
5		446.197	7.110(3)	452.658	1.268(9)
	Theory			453.468[a]	2.64(9)[a]
6		657.394	2.276(4)	665.436	1.703(9)
7		909.475	9.158(4)	919.113	2.409(9)
8		1202.496	2.497(5)	1213.744	3.117(9)
9		1536.491	6.060(5)	1549.366	3.918(9)
	Theory	1538.148[b]		1551.031[b]	
	Expt.	1535.48[b]		1550.84[b]	
10		1911.507	1.343(6)	1 926 027	4.813(9)
	Theory			1928.844[a]	1.269(10)[a]
				1924[c]	4.514(9)[c]
12		2784.820	5.332(6)	2802.706	6.899(9)
	Theory			2798[c]	6.619(9)[c]
14		3822.746	1.715(7)	3843.901	9.391(9)
	Theory			3835[c]	9.125(9)[c]
18		6396.059	1.138(8)	6424.385	1.568(10)
	Theory			6399[c]	1.534(10)[c]
	Expt.	6390[d]			
20		7933.026	2.491(8)	7967.522	1.945(10)
	Theory			7978.211[a]	5.56(10)[a]
22		9635.396	4.986(8)	9674.753	2.368(10)
26		13553.011	1.599(9)	13604.082	3.342(10)
	Theory			13625.14[a]	9.42(10)[a]

[a]Reference [31].
[b]Reference [20].
[c]Reference [32].
[d]Reference [11].

and two electron functions with angular correlation and orbital relaxation. Our calculated x-ray rates differ substantially from the results of Safronova *et al.* [31]. In general there is a good agreement between the present rates and the velocity gauge rates of Mukherjee *et al.* [32] with a deviation of 3 to 6% and the relativistic higher order corrections mainly account for the discrepancies between the two results.

Correlation correction very marginally decreases the allowed E1 energies of TEOP transitions. However, it increases the spin-forbidden energies by maximum of 0.3 eV. The Breit and QED contributions to TEOP energies are negligible for low Z ions and increase slowly with Z. At $Z = 26$, the decrease in MCDF energies due to Breit interaction and self energy corrections are 6 and ∼8 eV, respectively. As the nature of contributions from Breit and QED corrections are nearly the same for both allowed and forbidden transitions, the Breit interaction and self energy corrections to MCDF energies of $^1P_1$-$^1S_0$ transition are shown in Fig. 5.

Our calculations show that the contribution from large correlation functions (1094 CSFs) with respect to limited 24 CSFs set to the allowed E1 rates reduces the velocity gauge rates and increases the length gauge rates substantially. To analyze the importance of Breit interaction on the length and velocity forms of TEOP transition rates, in Fig. 6 we display the percentage variations in the rates of the allowed dipole lines from Breit interaction to the length and velocity form rates calculated with large orbital set. Unlike correlation contribution, the Breit interaction reduces the E1 rates of length and velocity gauges. It is seen from the figure that the influence of Breit interaction on the velocity gauge is nearly the same as that on the length gauge and the maximum contributions to velocity and length gauges rates are ∼16 and 14%, respectively, at $Z = 26$.

Radiative rates unlike energy levels are sensitive to the long-range behavior of atomic wavefunctions. While the correlation corrections are small for OEOP transitions and hence the treatment of OEOP transition rates needs only a comparatively lesser number of configurations to include the most relevant contributions to obtain the well-converged MCDF results, the TEOP transitions being extremely correlation sensitive, even though the orbital set with $n < 9$ and large angular correlation up to $l = 3$ gives well-converged values, the length gauge rates exceed the velocity gauge rates by 26% at $Z = 4$ to 35% at $Z = 26$. Residual contributions from higher partial waves with $l > 3$ are found to be negligible and do not reduce the differences between the length and velocity gauges rates. While the length and velocity gauges rates of OEOP transitions are gauge-independent, the strong gauge dependence of the competing TEOP rates might indicate the importance of negative energy states, which are omitted in the present

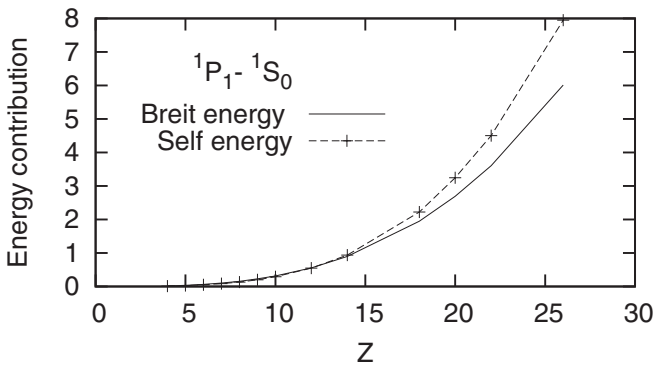

FIG. 5. Breit and self energy correction to the $2s2p\ ^1P_1$-$^1S_0$ transition energies in eV for various He-like ions.

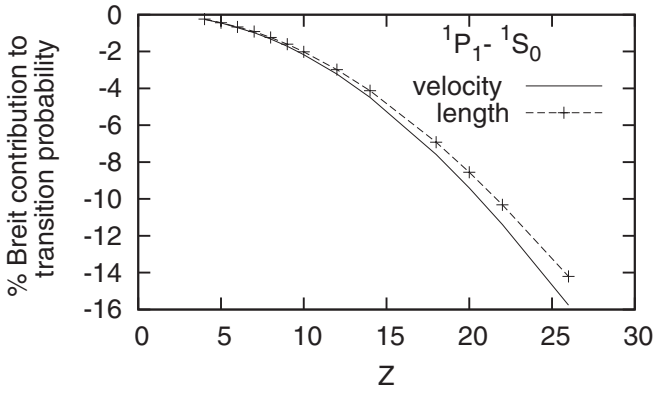

FIG. 6. Breit contribution to transition rates of $2s2p\ ^1P_1$-$^1S_2$ -$^1S_0$ transition in He-like ions.

calculations. An approximate estimate of the missing negative energy contribution in terms of $(Z\alpha)^2$ scaling leads to a difference of 5 to 6% between the computed A_l and A_v. Also, the present work takes only a partial account of Breit interaction as only the mixing coefficients are recalculated. Inclusion of Breit interaction in the self-consistent field calculation would alter the orbital shapes and though these modified spinors may have little effect on the transition energies, they may substantially influence the TEOP transition rates. We expect that such a treatment would eventually help in reducing the discrepancy between the length and velocity gauges rates.

TABLE V. The percentage errors in computed transition rates, line strengths, and transition energies. The first line gives the differences between the RCI rates (A) in length form and the energy scaled length form rates (A'). The second line shows the errors (δS) in line strengths calculated relative to the average of S_l and S_v and the third line lists the differences (δE) between the calculated and experimental transition energies. The numbers within the brackets denote powers of ten.

	Percentage error			
	$2s2p$-$1s2s$		$2s2p$-$1s^2$	
Property	$^1P_1$-$^1S_0$	$^3P_{0,1,2}$-$^3S_1$	$^1P_1$-$^3S_1$	$^1P_1$-$^1S_0$
		$Z=4$		
(A−A′)	+3.11(−1)	−7.78(−3)	+2.05(−1)	−4.92(−1)
δ S	+0.46	+0.15	+4.78	
δ E	+3.3(−2)	−1.27(−3)	+7.21(−2)	−0.16
		$Z=5$		
(A-A')	−1.71(−1)	−2.13(−2)	−6.91(−2)	−4.32(−1)
δS	+0.59	+0.03	+2.09	+3.37(+1)
δE	−5.66(−2)	−9.66(−3)	−2.35(−2)	−0.15
		$Z=6$		
(A-A')	−2.21(−2)	−4.00(−2)	+6.13(−2)	−2.39(−1)
δS	+0.54	+7.17(−3)	+1.24	+3.65(+1)
δE	−9.04(−3)	−1.65(−2)	+1.89(−2)	−7.99(−2)
		$Z=7$		
(A-A')	−1.30(−1)	−6.40(−2)	−5.59(−2)	−2.36(−1)
δS	+0.47	+2.12(−2)	+0.61	+3.84(+1)
δE	−4.42(−2)	−3.18(−2)	−2.02(−2)	−7.89(−2)
		Z = 8		
(A-A')	−4.30(−2)	−6.47(−2)	+1.55(−2)	−1.48(−1)
δS	+0.39	+3.41(−2)	+0.55	+3.98(+1)
δE	−1.64(−2)	−3.61(−2)	+3.74(−3)	−4.96(−2)
		$Z=9$		
(A-A')	−1.77(−3)	+6.75(−2)	+7.59(−2)	−7.61(−2)
δS	+0.32	+4.39(−2)	+0.43	+4.09(+1)
δE	−2.82(−3)	+3.06(−3)	+2.38(−2)	−2.62(−2)
		$Z=12$		
(A-A')	+2.50	−8.31(−2)	+2.55	+1.30
δS	+0.19	+4.66(−2)	+0.28	+4.28(+1)
δE	+8.46(−1)	−4.77(−3)	+8.57(−1)	+4.35(−1)
		$Z=14$		
(A-A')	−3.90(−2)	−4.82(−2)		
δS	+0.12	+3.51(−2)	+0.21	+4.34(+1)
δE	−1.31(−2)	−1.70(−2)		
		$Z=26$		
(A-A')	−1.94(−1)	+5.01(−1)		
δS	+0.08	+6.63(−2)	+2.00(−3)	+4.41(+1)
δE	−6.46(−2)	+1.69(−1)		

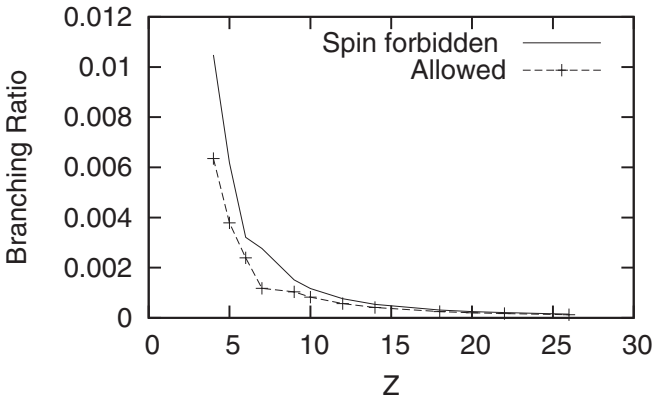

FIG. 7. Branching ratios of double- and single-electron radiative transitions.

While factors like convergence of the line strengths and agreement between the calculated and experimental transition energies and between A_l and A_v values give an overall indication on the accuracy of our results, we have also tried to critically evaluate the uncertainty in our computed rates. The accuracy of the calculated rates depends both on the line strengths and on the transition energies. In the evaluation of relative errors on transition energies δE, we have used the level energies listed in Table I for $Z \leqslant 12$. The experimental level energies for $1s2s\ ^1S_0$ state of $Z > 12$ could not be obtained, as observed data on $1s2s$ ($^1S_0$)-$1s^2$ ($^1S_0$) transition are not available; hence, we have used the transition energies listed in Table II. The uncertainties δS in the length (S_l) and velocity (S_v) forms of line strengths are calculated relative to the average of S_l and S_v values. If A is the RCI rate and A′ is the rate calculated using the observed transition energies and computed line strengths, then the uncertainty (δA) in our computed rate is (A-A'). The uncertainty estimates δE, δS, and δA for a few selected ions are listed in Table V for electric dipole allowed OEOP and TEOP transitions and also for $^1P_1$-$^3S_1$ spin-forbidden transition. It is seen from Table V that the relative error in the transition energies is within a fraction of a percent and the relative difference in the length and velocity forms of line strengths is well below 0.5% for the allowed OEOP transition. The discrepancy in the spin-forbidden line strength is within 1% except for He-like Be, B, and C. While the relative error in the TEOP transition energies is within 0.1%, the discrepancy in the line strengths is large; hence, the uncertainty estimate, which is the sum of the percentage error in transition energy and the percentage difference in the length and velocity forms of line strength, is as large as 40%.

In order to see the behavior of the TEOP transitions with respect to OEOP transitions, we have plotted in Fig. 7 the branching ratios between the two transitions for various Z. It is clear from the figure that the contribution from double-electron transition to the total radiative probability is appreciable for low Z ions.

IV. CONCLUSION

We have calculated the probabilities for the one- and two-electron radiative transitions from states of $2s2p$ configuration

to empty K shell in He-like ions and we find that the contribution from TEOP transition is appreciable for light ions. The influence of configuration interaction on single-electron allowed E1 transitions is marginal; hence, nonrelativistic calculations in intermediate coupling may be sufficient for low-Z elements. However, for the spin-forbidden transitions and double-electron jump into empty K shell, contributions from correlation and Breit interaction are appreciable and relativistic configuration interaction calculations are necessary. We have provided the error estimates for both OEOP and TEOP transition rates. As experimental results for TEOP transitions are currently nonexistent, we hope that our results will provide specific predictions for comparison with future experiments.

ACKNOWLEDGMENT

This work was performed under Project No. SR/S2/LOP-10 of 2007, funded by the Department of Science and Technology, Government of India.

[1] J. Hoszowska *et al.*, Eur. Phys. J Special Topics **169**, 23 (2009).
[2] J. Hoszowska, J. C. Dousse, J. Szlachetko,Y. Kayser, W. Cao, P. Jagodzinski, M. Kavcic, and S. H. Nowak, Phys. Rev. Lett. **107**, 053001 (2011).
[3] U. Feldman *et al.*, Astrophysics J. **192**, 213 (1974).
[4] E. V. Aglitskii *et al.*, Sov. J. Quantum Electron. **4**, 500 (1974).
[5] P. Nicolosi and G. Tondello, J. Opt. Soc. Am. **67**, 1033 (1977).
[6] E. T. Kennedy and P. K. Caroll, J. Phys. B **11**, 965 (1978).
[7] Takako Kato, Norimasa Yamamoto, and Frank Rosmej, Laser Part. Beams **22**, 245 (2004).
[8] Peter Hakel, R. C. Mancini, J. C. Gauthier, E. Minguez, J. Dubau, and M. Cornille, Phys. Rev. E **69**, 056405 (2004).
[9] N. Yamamoto, T. Kato, and F. Rosmej, J. Quantum Spectrosc. Radiat. Transfer **96**, 343 (2005).
[10] N. Yamamoto, T. Kato, and F. Rosmej, J. Plasma Fusion Res. Series **7**, 131 (2006).
[11] H. Tawara and P. Richard, Can. J. Phys. **80**, 1579 (2002).
[12] Ajay Kumar *et al.*, Nucl. Instrum. Methods Phys. Res., Sect. B **248**, 247 (2006).
[13] T. Nandi, Astrophys. J. **673**, L103 (2008).
[14] E. Kroupp *et al.*, IEEE **1**, 209 (2003).
[15] J. G. Lunney and J. F. Seely, Phys. Rev. Lett. **46**, 342 (1981).
[16] J. F. Seely and J. G. Lunney, Optic Comm. **41**, 43 (1982).
[17] E. Trabert, Can. J. Phys. **80**, 1481 (2002).
[18] B. E. O'Rourke *et al.*, Phys. Rev. A **77**, 062709 (2008).
[19] M. Bitter *et al.*, Phys. Rev. A **29**, 661 (1984).
[20] E. Trabert, B. E. Fawcett, and J. D. Silver, J. Phys. B **15**, 3587 (1982).
[21] J. P. Mosnier *et al.*, J. Phys. B **19**, 2531 (1986).
[22] K. J. H. Phillips, Astrophys. J. **605**, 921 (2004).
[23] M. H. Chen, Phys. Rev. A **38**, 3280 (1988).
[24] F. F. Goryayev and L. A. Vainshtein, e-print arXiv:physics/0603164v2 [physics.atom-ph] (2006).
[25] M. Deutsch and M. Hart, Phys. Rev. A **34**, 5168 (1986).
[26] S. Andriamonje, H. J. Andra, and A. Simionovici, Z. Phys. D **21**, S349 (1991).
[27] R. Hutton, P. Beiersdorfer, A. L. Osterheld, R. E. Marrs, and M. B. Schneider, Phys. Rev. A **44**, 1836 (1991).
[28] Y. Zou, J. R. Crespo Lopez-Urrutia, and J. Ullrich, Phys. Rev. A **67**, 042703 (2003).
[29] J. R. C. Lopez-Urrutia *et al.*, Nucl. Instrum. Methods Phys. Res., Sect. B **235**, 85 (2005).
[30] R. C. Etlon *et al.*, J. Quantum Spectrosc. Radiat. Transfer **65**, 185 (2000).
[31] U. I. Safronova and V. S. Senashenka, J. Phys. B **10**, L271 (1977).
[32] T. K. Mukherjee, T. K. Ghosh, and P. K. Mukherjee, Z. Phys. D **33**, 7 (1995).
[33] P. Jonsson, X. He, C. Froese Fischer, and I. P. Grant, Comput. Phys. Commun. **177**, 597 (2007).
[34] F. A. Parpia, C. Froese Fischer, and I. P. Grant, Comput. Phys. Commun. **94**, 249 (1996).
[35] W. R. Johnson and G. Soff, At. Data Nucl. Data Tables **33**, 405 (1985).
[36] L. Wayne Fullerton and G. A. Rinker, Phys. Rev. A **13**, 1283 (1976).
[37] I. P. Grant *et al.*, Comput. Phys. Commun. **21**, 207 (1980).
[38] B. J. Mckenzie, I. P. Grant, and P. H. Norrington, Comput. Phys. Commun. **21**, 233 (1980).
[39] I. P. Grant, *Relativistic Quantum Theory of Atoms and Molecules: Theory and Computation* (Springer, New York, 2007).
[40] L. Natarajan, J. Phys. B **35**, 3179 (2002).
[41] R. Kadrekar and L. Natarajan, J Phys. B **43**, 155001 (2010).
[42] On-line biblioghraphic database at NIST http://physics.nist.gov/asd3.